applied sciences

MDPI

Article

Spherical vs. Plane Lenses for Enhanced DUV-LED Performance and Wine Aging

Jichen Shen [1], Tianqi Wu [1], Jun Zou [1,*], Peng Wu [2] and Yitao Liao [2]

[1] School of Science, Shanghai Institute of Technology, Shanghai 201400, China; 236182109@mail.sit.edu.cn (J.S.); 236182116@mail.sit.edu.cn (T.W.)
[2] Liyu Advanced Technology Co., Ltd., Xuzhou 221116, China; pw@liyusemi.cn (P.W.); liao@liyusemi.cn (Y.L.)
* Correspondence: zoujun@sit.edu.cn; Tel.: +86-19821996286

Abstract

The strategic selection of lens geometry—spherical versus plane—decisively shapes the opto-thermal performance boundary of deep ultraviolet light-emitting diodes (DUV-LEDs), thereby governing their efficacy in application-specific photochemical processes. This study demonstrates that spherical lenses, by virtue of their superior light-collecting geometry, significantly enhance optical extraction efficiency and thermal management performance compared to conventional plane lenses. These engineered performance characteristics translate directly into divergent functional outcomes: spherical lenses enable rapid, high-intensity processing, while plane lenses are better suited for controlled, sustained operation. The findings establish a fundamental principle for DUV-LED packaging design: lens geometry can be tailored to optimize efficiency for distinct photochemical tasks, providing a clear pathway from device engineering to application-driven performance.

Keywords: deep ultraviolet light; plane lens; spherical lens

1. Introduction

Deep ultraviolet light-emitting diodes (DUV LEDs) demonstrate considerable application potential across multiple fields, including sterilization, biochemical sensing, water treatment, and air purification. Nevertheless, their broader adoption is impeded by two persistent technical challenges: limited light extraction efficiency and insufficient thermal management.

Optically, while conventional quartz glass encapsulation is necessary for durability, its geometry critically determines the effectiveness of light extraction. Conventional planar windows fail to effectively collect the highly divergent emission from DUV LED chips, trapping a significant portion of light within the package and severely constraining external quantum efficiency [1–5]. Electrically, DUV LEDs typically exhibit a low electro-optical conversion efficiency of only 15–25%, with the remainder of input power being dissipated as heat, thereby making thermal management a crucial determinant of device performance and operational reliability [6,7]. The thermal behavior of DUV LEDs critically governs their long-term reliability. Elevated junction temperatures not only diminish optical output but also accelerate device aging and may induce irreversible degradation. As an integral element of the packaging architecture, the lens design governs both optical field distribution and thermal resistance characteristics [8,9]. Previous studies have established a positive correlation between packaging thermal resistance and junction temperature, identifying thermal resistance as a key factor influencing LED service life. Thus, minimizing thermal

Academic Editor: Ephraim Suhir

Received: 26 November 2025
Revised: 21 January 2026
Accepted: 22 January 2026
Published: 24 January 2026

resistance and optimizing heat dissipation pathways have emerged as central research priorities [10,11]. In line with this principle, this work systematically examines the influence of spherical and plane lens configurations on the photothermal performance of DUV LEDs.

Based on the foregoing understanding, this study proposes an overarching hypothesis: The strategic selection of lens geometry (spherical versus plane) enables the optimization of opto-thermal parameters within a DUV-LED system. This optimized opto-thermal performance profile is posited to directly determine the efficiency and quality of specific photochemical maturation processes. Specifically, the intrinsic geometric differences between spherical and plane lenses are expected to induce differential modulation of the DUV-LED's optical output intensity and junction temperature. These unique combinations of opto-thermal parameters are then hypothesized to align with the distinct demands of different photochemical maturation applications, such as achieving rapid oxidative maturation or facilitating gradual, controlled aging.

To test this hypothesis, the present study is structured into two coherent and logically sequential phases. First, we systematically investigate the influence of spherical versus plane lens geometries on the optical output intensity and thermal performance of DUV-LEDs, with the objective of identifying packaging solutions that synergistically enhance both light output and thermal management. This phase encompasses a comparative analysis of photothermal performance and a 1000-h accelerated aging test designed to evaluate device reliability and elucidate degradation mechanisms.

Subsequently, to demonstrate how this engineered opto-thermal performance envelope directly dictates application outcomes, we employ the characterized DUV-LEDs in a model photochemical process: the accelerated aging of yellow wine. Contemporary mainstream aging technologies have evolved along two primary trajectories. The first is traditional pottery jar aging. As a classical technique, this method relies on the microporous structure of the clay jar to facilitate slow gas exchange between the wine and its environment, thereby developing a rich and mellow flavor profile over months or even years of natural storage. However, this process is significantly constrained by its prolonged duration, substantial spatial requirements, high cost, and susceptibility of product quality stability to environmental factors [12,13]. The second trajectory is modern accelerated aging technology, which aims to overcome the bottlenecks of traditional methods. For instance, biological modulation approaches are employed, involving the inoculation of selected functional microorganisms (e.g., specific yeasts, esterifying bacteria) or the addition of exogenous enzymatic preparations to directionally catalyze the synthetic pathways of specific flavor compounds, thereby achieving controlled flavor development and a shortened production cycle. Nevertheless, existing acceleration techniques predominantly focus on regulating biochemical processes and lack a precise means for the selective excitation of photosensitive components in wine using high-energy photons [14,15]. This identified gap provides an ideal testbed for validating our core hypothesis.

Therefore, by utilizing DUV-LEDs operating at 255 nm, 265 nm, and 275 nm in conjunction with both optical configurations, we systematically investigate their aging effects on yellow wine. The experimental results confirm that DUV treatment can rapidly impart sensory attributes characteristic of traditionally aged wine to fresh samples, thereby offering an efficient and innovative aging technology. Through this approach, we successfully establish a direct correlation between the lens-governed opto-thermal properties and their efficacy in specific applications.

2. Materials and Methods

This study systematically evaluated the key performance metrics of deep ultraviolet light-emitting diodes (DUV-LEDs) (Shenzhen Ruibao Light Technology Co., Ltd., Shenzhen,

China) operating at three distinct wavelengths—255 nm, 265 nm, and 275 nm—including relative output intensity (arbitrary units, a.u.), junction temperature, and device reliability. For each wavelength, a comparative analysis was conducted between two lens packaging configurations: a plane lens and a spherical lens.

As shown in Figure 1, both packaging structures were fabricated on an aluminum nitride (AlN) ceramic substrate measuring 3.85 mm × 3.85 mm. The AlN ceramic substrate was selected primarily for its high thermal conductivity, which promotes efficient heat dissipation, as well as its excellent electrical insulation properties. The optical windows were fabricated from synthetic fused silica (Suprasil 3001 or equivalent grade), ensuring high transmittance (>90%) and excellent resistance to deep ultraviolet radiation. To achieve a precise physical interpretation and guarantee reproducibility, the following key geometric and optical parameters of the lenses are specified: the plane lens is a plano-parallel window with a thickness of 1.0 mm; the spherical lens is a plano-convex hemispherical lens with a radius of curvature (ROC) of 1.5 mm and a center thickness of 3.0 mm, resulting in the final package height illustrated in Figure 1b. Furthermore, a broadband anti-reflection (AR) coating optimized for the 250–280 nm spectral range was applied to the exterior (air-facing) surface of both lens types. This coating reduces the Fresnel reflection loss at each lens–air interface to below 1%, thereby equalizing and minimizing this loss factor across the two comparative lens configurations. This controlled condition allows the subsequent analysis to focus specifically on the effects arising from the intrinsic geometric differences between the lenses.

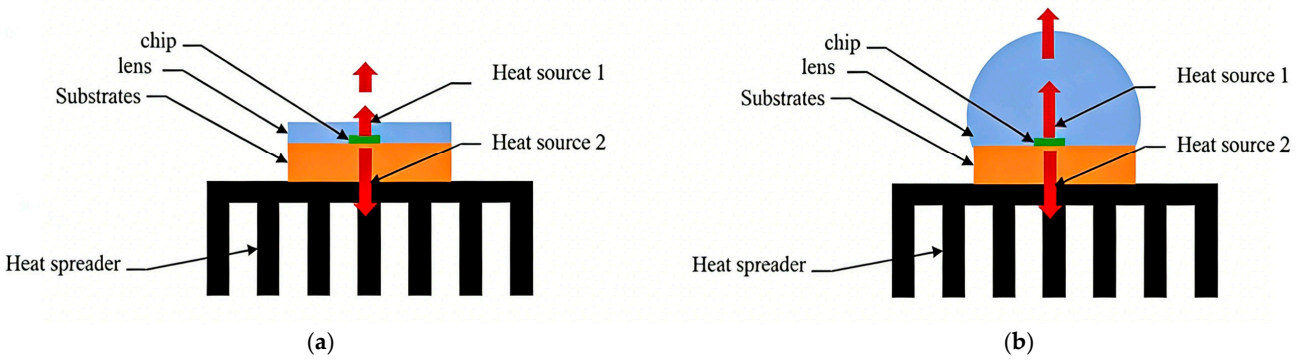

Figure 1. Schematic diagrams of DUV-LED packaging configurations. (**a**) Spherical lens packaging: Plano-convex hemispherical lens (ROC = 1.5 mm) bonded to AlN substrate via UV-resistant silicone; (**b**) Plane lens packaging: Plano-parallel window (thickness = 1.0 mm) with identical sealing and substrate parameters. Heat 1: Heat from the chip → lens → surface air convection, which typically accounts for less than 10% of the total heat dissipation. Heat 2: chip-generated heat → aluminum nitride ceramic substrate → thermal interface material → heat sink → ambient air.

To ensure the hermeticity and long-term reliability of the package, a high-purity, deep-ultraviolet-resistant silicone material was employed as the sealing medium to achieve a hermetic bond between the quartz glass lens and the AlN ceramic substrate.

To mitigate the risk of thermal degradation during extended operation, all LED devices were thermally bonded to aluminum heat sinks (40 × 40 × 11 mm) using STARS-992 high-performance thermal adhesive. The adhesive was cured at room temperature for four hours to form a stable mechanical and thermal interface, thereby ensuring consistent heat dissipation performance throughout the experiments. The junction temperature (T_J) was measured using an LEDT-300B/H integrated thermal management system—a setup specifically designed for the thermal characterization of LEDs—in conjunction with a UNI-T DC power supply, which provided driving currents in the range of 20–60 mA. The forward voltage method was employed for the measurements, leveraging the well-

defined negative temperature coefficient characteristic of semiconductor junctions. As the temperature increases, the forward voltage exhibits an approximately linear decrease, enabling accurate determination of the junction temperature. All thermal measurements were carried out inside a Date Compare environmental chamber, which maintained a stable ambient temperature of 25.0 ± 0.5 °C, thus ensuring the reproducibility and consistency of the experimental results.

Reliability assessments of the devices were carried out using an LR-253 constant temperature and humidity aging test chamber. The aging tests were performed under controlled environmental conditions of 25 °C and 50% relative humidity for a continuous duration of 1000 h. We measured the relative output intensity (arbitrary units, a.u.) of the DUV-LEDs using an FX4000-Ex high-resolution spectrometer. All devices were characterized under identical instrumental settings across the driving current range of 20–60 mA to ensure a valid comparative analysis.

For the Yellow Wine maturation investigation, Hua Diao Yellow Wine was selected as the sample matrix. The Yellow Wine samples were irradiated with deep ultraviolet light over periods of 10, 20, and 30 days using the previously described DUV-LED devices. Spectral changes throughout the aging process were monitored using an Edinburgh spectrometer. All spectral measurements were conducted under consistent experimental conditions to ensure reproducibility and to support an objective analysis of the effects of deep ultraviolet exposure on the maturation of Yellow Wine, thereby enabling scientifically robust conclusions.

3. Results and Discussion

3.1. Analysis of Optical Output from Different Lenses

In the packaging of deep ultraviolet light-emitting diodes (DUV-LEDs), the high energy of deep ultraviolet radiation precludes the use of organic encapsulation materials due to their rapid photodegradation. Fused silica (quartz) is therefore adopted as the encapsulation medium. To mitigate the Fresnel reflection losses inherent at any dielectric-air interface, a broadband anti-reflection (AR) coating was applied to the exterior surface of both lens types, reducing the reflectance to below 1% per surface across the 250–280 nm band.

Under this condition of equalized and minimized interfacial reflection, our experimental results reveal that packages employing spherical lenses consistently achieve a higher optical output compared to those with plane lenses. This demonstrates that the performance advantage of the spherical lens stems not from overcoming a reflection disadvantage, but from its intrinsic geometric superiority [16–18].

As illustrated in Figure 2a, two lens architectures—spherical and plane—were implemented in the DUV-LED packages in this study. The relative output intensity of both lens types was systematically evaluated under different drive currents using a spectrometer-based measurement system. Experimental data show that as the drive current was incrementally raised from 20 mA to 60 mA, all tested DUV-LED devices exhibited a consistent and notable increase in output intensity across the three emission wavelengths.

Specifically, at a wavelength of 255 nm, the relative intensity of the spherical-lens device increased from 25,000 a.u. to 65,000 a.u., whereas that of the plane-lens device rose from 20,000 a.u. to 59,000 a.u. At 265 nm, the spherical-lens configuration showed an increase from 25,000 a.u. to 58,000 a.u., compared to an increase from 17,000 a.u. to 55,000 a.u. for the plane lens. At 275 nm, the spherical lens exhibited an intensity rise from 22,000 a.u. to 59,000 a.u., while the plane lens increased only from 17,000 a.u. to 51,000 a.u.

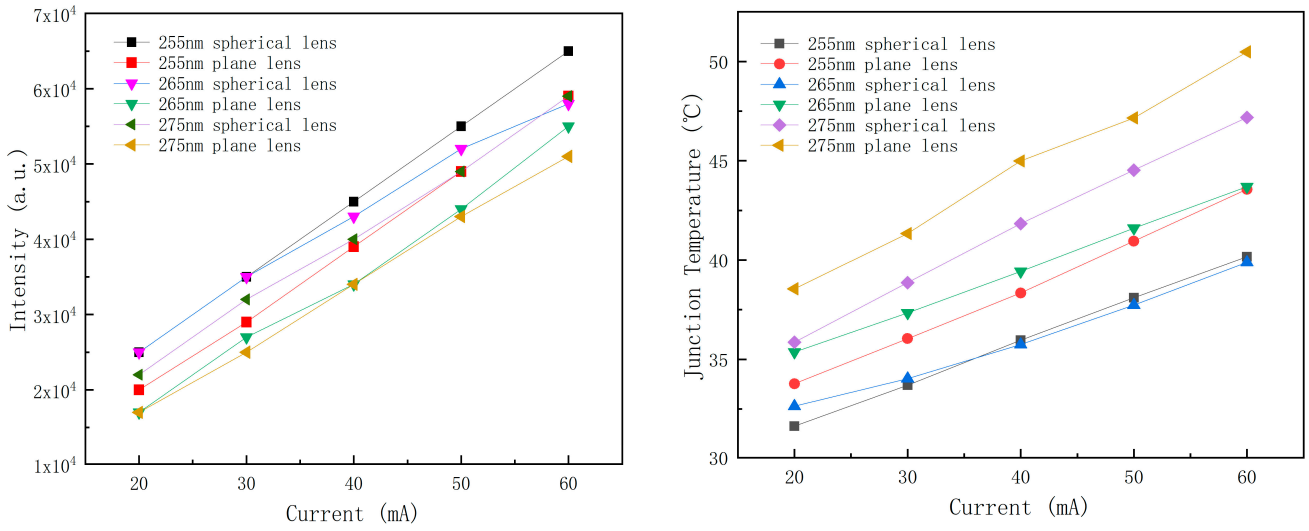

(**a**) (**b**)

Figure 2. Opto-thermal performance of DUV-LEDs with spherical and plane lenses. (**a**) Relative output intensity (a.u.) as a function of driving current (20–60 mA) at 255 nm, 265 nm, and 275 nm; (**b**) Junction temperature (T_J, °C) as a function of driving current (20–60 mA) at the same wavelengths.

Notably, the enhancement in optical output provided by the spherical lens was most pronounced at 265 nm. At a drive current of 30 mA, the intensity difference reached a maximum of 9000 a.u., underscoring the superior optical output performance of the spherical lens at this specific wavelength.

A comprehensive analysis confirms that across the three representative DUV wavelengths, devices packaged with spherical lenses consistently achieve higher relative output intensities (a.u.) than those with plane lenses. Under identical operating conditions, the spherical lens provides a minimum enhancement of 25% in relative intensity compared to the plane lens. This improvement is primarily attributed to the superior light-collecting capability of the spherical lens. Its curved surface and higher effective numerical aperture allow it to capture and redirect a larger portion of the chip's highly divergent emitted light, thereby improving the overall coupling efficiency of light out of the package. the dominant mechanism for the observed signal enhancement is the enhanced light extraction geometry of the spherical lens itself.

3.2. Analysis of Operating Junction Temperatures for Different Lenses

This study presents a systematic comparative analysis of the thermal characteristics of deep ultraviolet light-emitting diode devices operating at three distinct wavelengths: 255 nm, 265 nm, and 275 nm. As shown in Figure 2b, a consistent upward trend in junction temperature was observed across all device configurations as the drive current was increased from 20 mA to 60 mA. The detailed results are summarized as follows: at 255 nm, the junction temperature of spherical-lens packaged devices increased from 31.63 °C to 40.17 °C, while that of plane-lens devices rose from 33.77 °C to 43.56 °C; at 265 nm, the junction temperature of spherical-lens devices increased from 32.64 °C to 39.88 °C, compared to an increase from 35.37 °C to 43.69 °C for plane-lens devices; at 275 nm, spherical-lens devices exhibited a temperature increase from 35.86 °C to 47.18 °C, whereas plane-lens devices showed a rise from 38.55 °C to 50.48 °C.

These results indicate that under identical operating currents, devices packaged with spherical lenses consistently maintain junction temperatures approximately 2–3 °C lower than those equipped with plane lenses. This measurable temperature reduction

underscores the superior thermal management performance afforded by spherical lens encapsulation—a particularly vital advantage in high-power DUV-LED applications, where efficient heat dissipation is essential for ensuring sustained device performance and long-term operational reliability.

The thermal resistance of different packaging structures was quantified by integrating measured electrical power data with substrate surface temperature (T_C), monitored via thermocouple, using the standard formula $Rth = (T_J - T_C)/P$. Here, T_J is the junction temperature and P denotes the total input electrical power dissipated as heat. As summarized in Tables 1–4, which present representative data for 255 nm and 265 nm devices, the thermal resistance of both configurations exhibited a decreasing trend as the current increased from 20 mA to 60 mA. Notably, under equivalent wavelength and current conditions, spherical lens packaging consistently demonstrated lower thermal resistance values than plane lens packaging.

Table 1. 255 nm spherical deep ultraviolet lamp bead test data.

Current (mA)	Voltage (V)	Power (W)	T_J (Junction Temperature) (°C)	T_C (Substrate Temperature) (°C)	Thermal Resistance (°C/W)
20	5.307	0.104	31.63	26.32	51.06
30	5.398	0.157	33.7	26.97	42.87
40	5.475	0.217	35.96	27.45	39.22
50	5.546	0.275	38.1	27.96	36.87
60	5.61	0.334	40.17	28.32	35.48

Table 2. 255 nm plane deep ultraviolet lamp bead test data.

Current (mA)	Voltage (V)	Power (W)	T_J (Junction Temperature) (°C)	T_C (Substrate Temperature)	Thermal Resistance (°C/W)
20	5.513	0.108	33.77	26.29	69.26
30	5.625	0.167	36.04	27.12	53.41
40	5.711	0.226	38.34	28.13	45.18
50	5.779	0.287	40.95	29.18	41.01
60	5.837	0.348	43.56	30.02	38.91

Table 3. 265 nm spherical deep ultraviolet lamp bead test data.

Current (mA)	Voltage (V)	Power (W)	T_J (Junction Temperature) (°C)	T_C (Substrate Temperature)	Thermal Resistance (°C/W)
20	5.684	0.116	32.64	26.86	49.83
30	5.778	0.172	34.03	27.7	36.80
40	5.847	0.231	35.75	28.71	30.48
50	5.901	0.292	37.73	30.03	26.37
60	5.946	0.353	39.88	31.22	24.53

Table 4. 265 nm plane deep ultraviolet lamp bead test data.

Current (mA)	Voltage (V)	Power (W)	T_J (Junction Temperature) (°C)	T_C (Substrate Temperature)	Thermal Resistance (°C/w)
20	5.778	0.119	35.37	26.28	76.39
30	5.886	0.176	37.34	26.95	59.03
40	5.972	0.237	39.43	27.74	49.32
50	6.042	0.299	41.6	28.63	43.38
60	6.099	0.363	43.69	29.39	39.40

The lower thermal resistance achieved with spherical lenses effectively suppresses heat accumulation during operation, thereby slowing performance degradation caused by temperature rise and contributing to improved device stability and extended service life. In summary, the spherical lens packaging configuration offers significant practical value for DUV-LED applications due to its superior thermal management capabilities.

Notably, although the absolute junction temperature difference is modest in magnitude, analysis based on the Arrhenius equation indicates that this 2–3 °C reduction can enhance device reliability by more than 15%. Furthermore, the spherical lens configuration achieves over 25% higher optical output power compared to the plane lens design. These results collectively demonstrate the superiority of spherical lenses in achieving enhanced optothermal synergy [19–21]. The simultaneous improvement in thermal management and light extraction efficiency renders spherical lenses a highly effective solution for elevating the overall performance of DUV LEDs, as corroborated by Arrhenius-based reliability modeling.

$$K = A \times e^{-E_a/(K_B T)} \quad (1)$$

where K is the degradation rate constant, A is the pre-exponential factor, Ea is the activation energy (in eV), K_B is the Boltzmann constant (8.617×10^{-5} eV/K), and T is the absolute junction temperature (in K).

Derivation based on the Arrhenius equation:

Assuming the activation energy of LED failure Ea ≈ 0.7 eV (a typical value), the acceleration factor for the device lifetime as the junction temperature decreases from T_1 to T_2 is given by:

$$\frac{L_2}{L_1} = e^{\frac{E_a}{K_B}\left(\frac{1}{T_1} - \frac{1}{T_2}\right)} \quad (2)$$

where L represents the mean time to failure (MTTF).

3.3. Reliability Analysis

This study conducted a 1000-h accelerated aging test on deep ultraviolet light-emitting diodes (DUV-LEDs) with emission wavelengths of 255 nm, 265 nm, and 275 nm under ambient conditions (25 °C). As shown in Figure 3, the relative output intensity of all devices increased approximately linearly with the drive current in the 20–60 mA range, with no signs of saturation observed. After aging, devices packaged with plane lenses showed a reduction in relative intensity of 4–20%, while those with spherical lenses exhibited a decrease of 6–22%. Although the spherical-lens devices initially delivered higher output intensity, their degradation rate was similar to that of the plane-lens devices. After 1000 h of aging, both packaging types demonstrated significant decay in optical performance, with no statistically significant difference in their degradation rates.

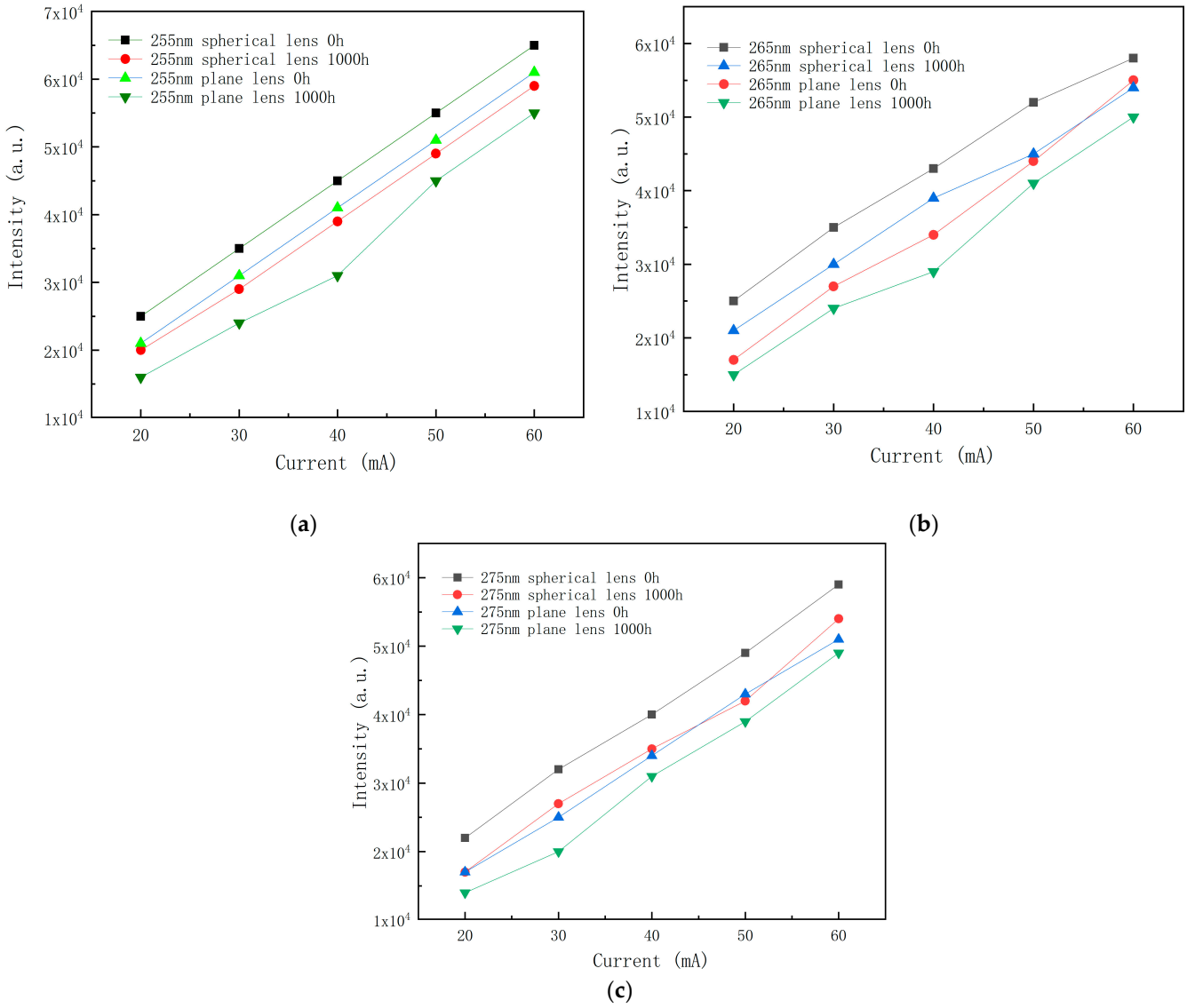

Figure 3. Relative output intensity of DUV-LEDs before and after 1000-h accelerated aging at (**a**) 255 nm, (**b**) 265 nm, and (**c**) 275 nm. Tests were conducted under constant conditions of 25 °C, 50% RH, and a driving current range of 20–60 mA.

Further investigation revealed that the decrease in output intensity is mainly caused by a progressive oxidation process at the electrode interface. Specifically, ambient oxygen (O_2) and water vapor (H_2O) penetrate the device through microstructural defects or sub-micron gaps in the encapsulation material. These species then engage in electrochemical oxidation reactions with the metal layers of the p-type electrode (e.g., Ni/Au or Pd/Ru), as exemplified by the representative reaction: $Ni + O_2 \rightarrow NiO_X$. This oxidation mechanism leads to an increase in interfacial state density and elevated contact resistance, ultimately resulting in the degradation of the device's optoelectronic performance [22–25].

This result carries important implications for long-term application and lens selection. It suggests that the optical output advantage of spherical lenses may gradually diminish over extended operational time if the hermeticity of the packaging is not further improved. Consequently, for applications requiring peak intensity over short- to medium-term durations, spherical lenses remain the optimal choice. In contrast, for applications prioritizing consistent output and minimal maintenance over very long lifetimes, plane lenses—with their slightly lower initial efficiency but more stable degradation trajectory—may offer a more reliable option.

Thermal performance analysis reveals that after 1000 h of aging at ambient temperature, deep ultraviolet LED devices with wavelengths of 255 nm, 265 nm, and 275 nm—packaged in both spherical and plane lens configurations—maintain excellent thermal stability across operating currents ranging from 20 to 60 mA. As illustrated in Figure 4, the junction temperatures measured at identical currents increased slightly across all devices following the aging process. However, this post-aging increase was minimal, ranging from 0 to 1 °C, which falls within the experimental measurement uncertainty of ±0.5 °C and was not statistically significant ($p > 0.05$). This consistent thermal behavior is attributed to the optimized thermal management design of the devices, which incorporates two key elements: first, a high-thermal-conductivity AlN ceramic substrate (κ = 170 W/m·K) serves as the primary heat-spreading material [26–28]; and second, an integrated high-efficiency heat sink structure is employed. Together, these components effectively mitigate heat accumulation. It is noteworthy that AlN exhibits high thermal stability—the 1000-h aging period at room temperature did not induce any substantial alteration in its crystal structure or thermal conductivity (rate of change < 1%) [29–32].

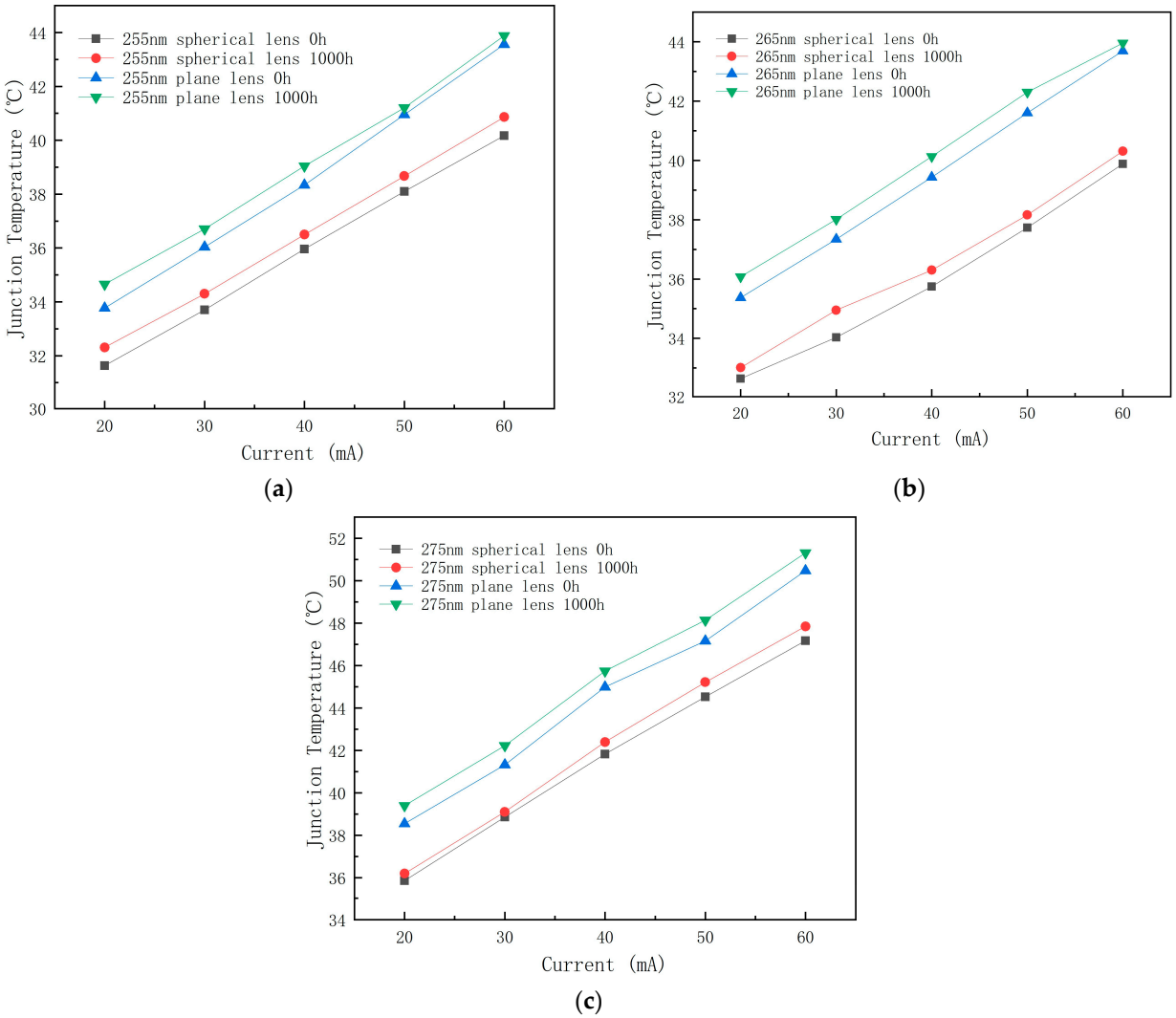

Figure 4. Junction temperature (T_J, °C) of DUV-LEDs before and after 1000-h accelerated aging. (**a**) 255 nm; (**b**) 265 nm; (**c**) 275 nm. Tests were conducted under constant conditions of 25 °C, 50% RH, and a driving current range of 20–60 mA.

These results clearly demonstrate that under the described experimental conditions, room-temperature aging primarily leads to a reduction in optical output power (4–22%)

in deep ultraviolet LEDs, without significantly impairing their thermal performance. The underlying reason is that aging at room temperature mainly affects the optoelectronic interfaces (such as through electrode oxidation), whereas critical thermal management components—namely the AlN substrate and heat sink—retain their structural and functional integrity throughout the aging process.

4. Aging Treatment Using Packaged Deep Ultraviolet LED

Based on the photothermal characteristics and reliability results presented in Sections 2 and 3, specific DUV-LED configurations were selected for the photochemical maturation experiments of yellow wine. Section 2 demonstrated that spherical lenses provide at least a 25% higher optical output than plane lenses at wavelengths of 255 nm, 265 nm, and 275 nm. All configurations also exhibited reliable thermal performance, with spherical lenses reducing the junction temperature by 2–3 °C. The 1000-h aging tests in Section 3 further confirmed excellent thermal stability and acceptable degradation rates for both lens types across all three wavelengths.

Yellow wine irradiation experimental model. The yellow wine irradiation model is shown in Figure 5. The experimental configuration was as follows: a 10.0 mL volume of Hua Diao yellow wine was sealed within a standard quartz cuvette with a 10 mm optical path length. A DUV-LED (packaged with a spherical or plane lens) was mounted on the inner surface of the cuvette cap, with a fixed distance of 5.0 mm maintained between the LED lens and the surface of the yellow wine solution. To isolate photochemical effects from confounding variables, the cuvette was sealed with a PTFE (polytetrafluoroethylene) liner and the entire assembly was placed inside a temperature-controlled incubator maintained at 25.0 ± 0.5 °C, thereby eliminating the influence of solvent evaporation and thermal fluctuations on the aging process.

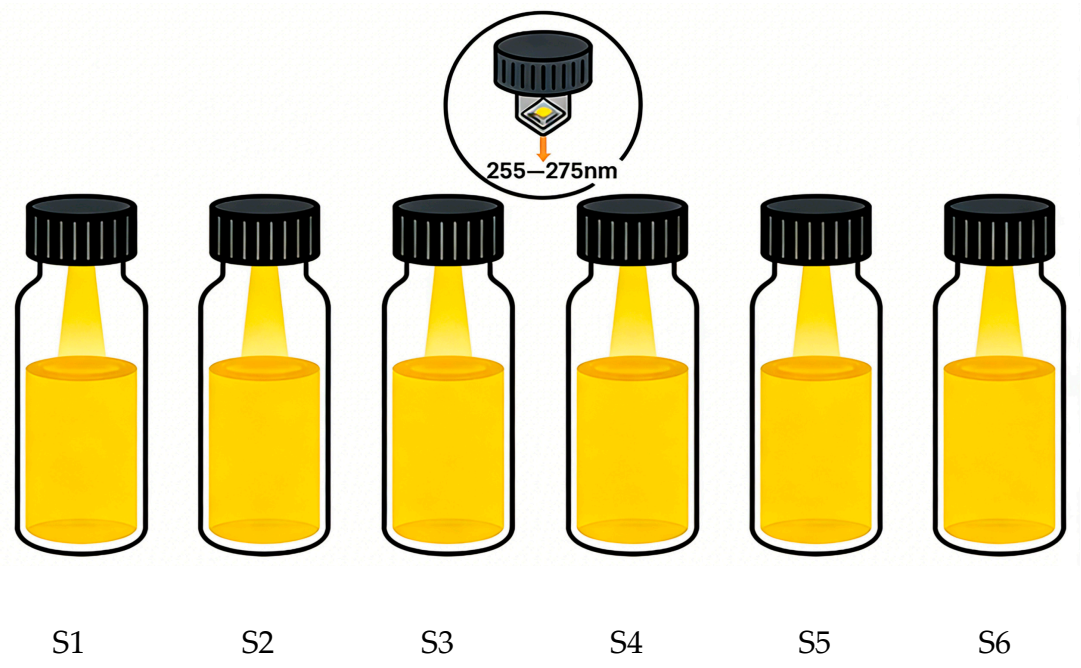

Figure 5. Yellow wine irradiation experimental model. Schematic of the DUV irradiation setup for yellow wine: 10.0 mL Hua Diao yellow wine sealed in a 10 mm optical path quartz cuvette. A DUV-LED (spherical/plane lens packaged) was mounted on the inner surface of the cuvette cap, maintaining a fixed distance of 5.0 mm from the yellow wine solution surface.

Consequently, DUV-LEDs operating at 255 nm, 265 nm, and 275 nm, each equipped with both spherical and plane lenses, were ultimately chosen as the irradiation sources. This

component selection, grounded in validated system performance, elevates the subsequent experiments from a standalone case study to a targeted and deliberate verification of suitability for the intended application.

This study was initiated with a systematic assessment of the feasibility of employing deep ultraviolet (DUV) radiation technology in the aging process of Yellow Wine. Yellow Wine, utilizing ultraviolet–visible (UV–Vis) absorption spectroscopy. As depicted in Figure 6a, the Yellow Wine samples demonstrated pronounced absorption within the ultraviolet spectrum below 360 nm, with a particularly strong and continuous absorption band observed between 200–280 nm. This spectral behavior indicates that several organic constituents in the Yellow Wine—such as phenolic compounds, carbonyl-containing molecules (e.g., aldehydes and ketones), and aromatic species—possess substantial absorption capacity within the DUV range. Such absorption is capable of inducing a series of photophysical and photochemical processes, including electron excitation, molecular dissociation, and free radical reactions. These results establish a theoretical basis for the subsequent use of DUV LED sources in achieving targeted and controlled aging processes.

Upon completion of the ultraviolet absorption characterization, a series of meticulously controlled experiments were designed to evaluate the influence of optical lens configurations on the efficiency of deep ultraviolet photocatalytic aging. Deep ultraviolet LEDs with three distinct central wavelengths (255 nm, 265 nm, and 275 nm) and two lens geometries (spherical and plane) were selected as irradiation sources. The experiments were conducted over three treatment durations—10 days, 20 days, and 30 days—to systematically investigate the temporal evolution of the chemical properties of Yellow Wine. To ensure a consistent baseline of total radiant energy across all comparative experiments, the irradiation procedures involved independently adjusting the driving current (or voltage) for each lens configuration so that the total optical power reaching the sample surface attained a pre-defined, unified standard. This calibration step effectively eliminated energy input disparities arising from inherent source efficiency variations. Consequently, any observed differences in aging outcomes can be directly and exclusively attributed to variations in the spatial distribution of photons—that is, the optical field—defined by the lens geometry.

The evolution of the characteristic emission peak at 460 nm under different lens types and treatment durations is shown in Figure 6b–d. For irradiation at 255 nm, the plane lens group exhibited emission intensities of 31,000 a.u., 32,500 a.u., 35,000 a.u., and 36,000 a.u. after 0, 10, 20, and 30 days of treatment, respectively. In comparison, the spherical lens group showed values of 31,000 a.u., 34,000 a.u., 37,000 a.u., and 34,500 a.u. under the same conditions. At 265 nm, the plane lens produced peak intensities of 31,000 a.u., 32,400 a.u., 34,000 a.u., and 36,500 a.u., whereas the spherical lens resulted in values of 31,000 a.u., 32,500 a.u., 37,250 a.u., and 33,000 a.u. Across the corresponding time points. For the 275 nm group, the plane lens yielded intensities of 31,000 a.u., 32,000 a.u., 34,000 a.u., and 36,000 a.u., compared to 31,000 a.u., 33,000 a.u., 40,000 a.u., and 35,000 a.u. for the spherical lens over the same period.

The data indicate that under identical wavelength and duration conditions, the spherical lens consistently produced higher peak intensities at 460 nm compared to the plane lens, corroborating its superior optical energy output. This enhanced energy correlates with increased photocatalytic reaction rates and more accelerated aging effects. The improvement is attributed to the superior focusing capability of the spherical lens, which elevates the energy density per unit area and promotes key photochemical pathways such as alcohol oxidation and esterification.

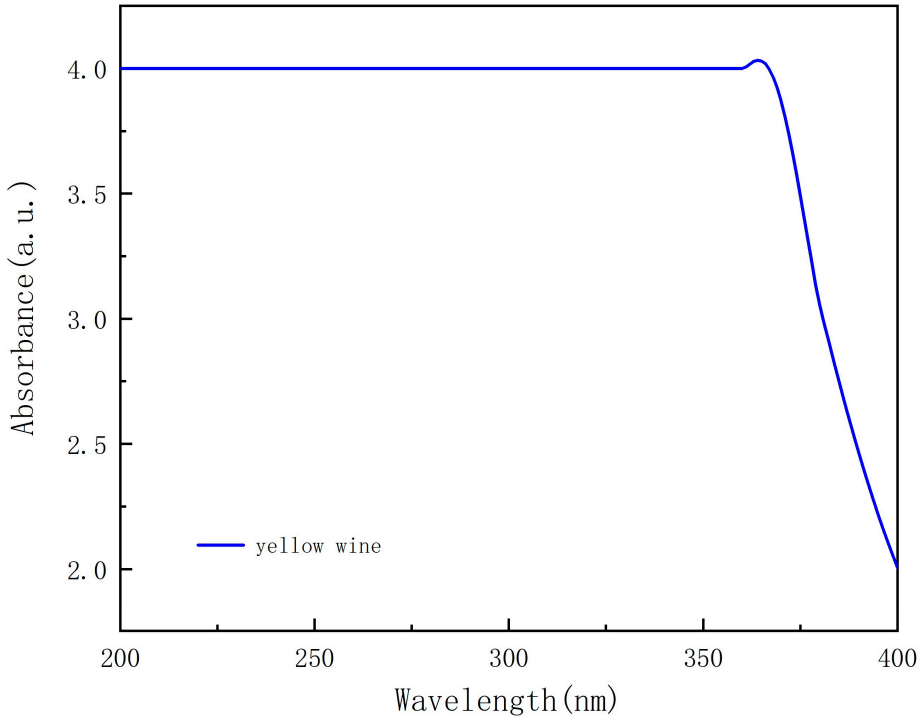

(**a**)

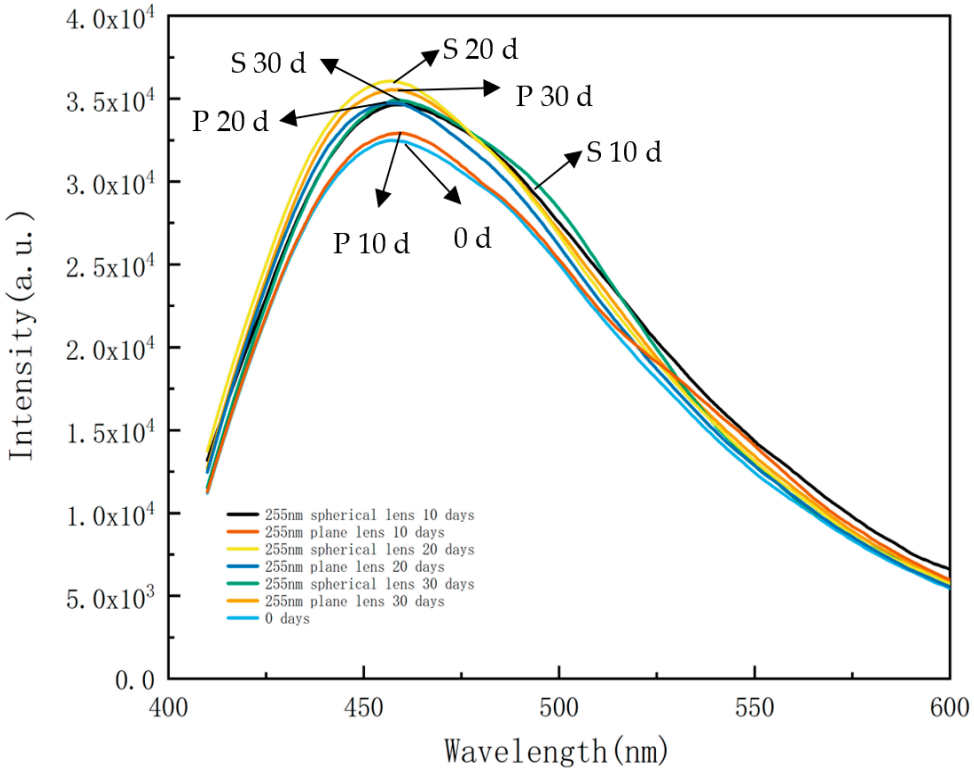

(**b**)

Figure 6. *Cont.*

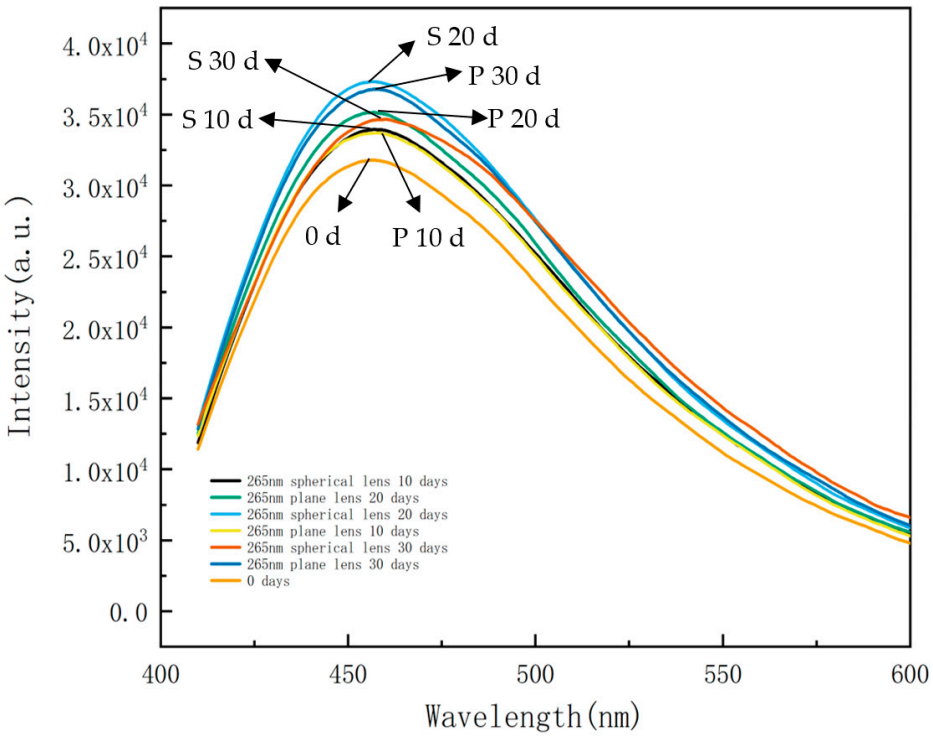

(**c**)

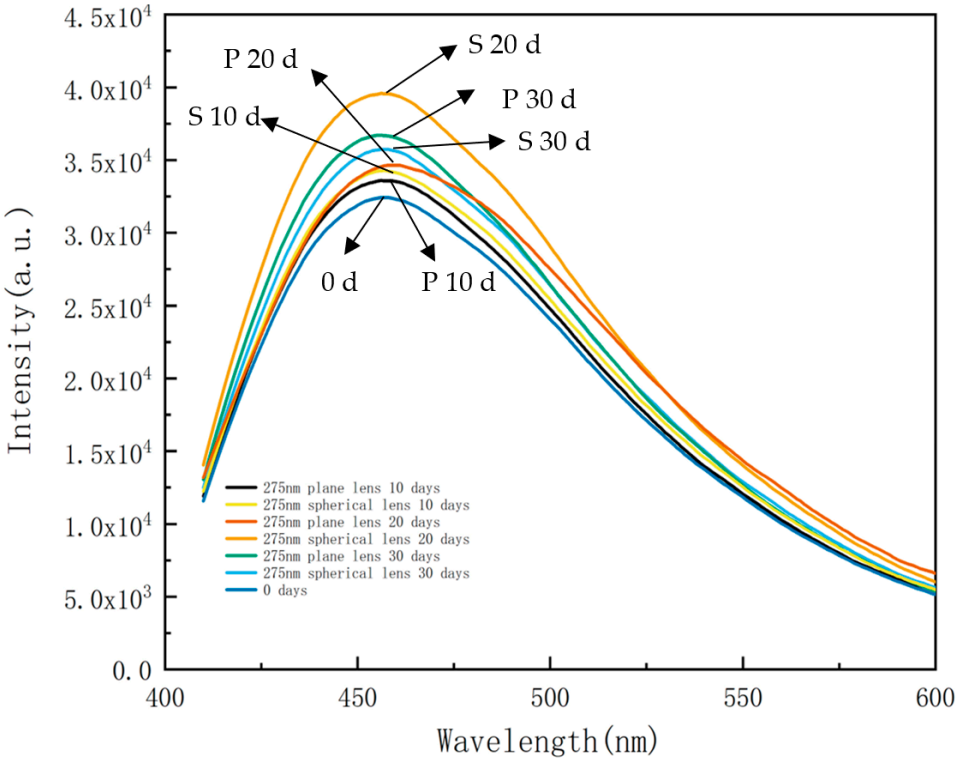

(**d**)

Figure 6. UV–Vis Absorption and Fluorescence Emission Spectra of Yellow Wine Before and After DUV-LED Irradiation.(**a**) UV–Vis absorption spectrum of unaged Hua Diao yellow wine (200–400 nm), showing strong ultraviolet absorption; (**b**–**d**) Fluorescence emission spectra of wine samples irradiated with 255 nm (**b**), 265 nm (**c**), and 275 nm (**d**) DUV-LEDs (spherical and plane lens packaged) for 0, 10, 20, and 30 days, respectively.

It is noteworthy that after 30 days of irradiation, all spherical lens groups exhibited a reduction in peak intensity: from 37,000 to 34,500 a.u. at 255 nm, from 37,250 to 33,000 a.u. at 265 nm, and from 40,000 to 35,000 a.u. at 275 nm. This suggests that prolonged high-energy exposure may lead to photodegradation or overoxidation of certain Yellow Wine components, ultimately counteracting the aging benefits. In contrast, the plane lens groups demonstrated a steady increase in signal intensity over the entire period, reflecting a more moderate and controllable photochemical process suitable for extended aging.

The mechanistic analysis indicates that these differences stem from the distinct photon flux distributions and energy transfer efficiencies associated with the two lens types. The spherical lens creates localized high-energy zones, which may facilitate the generation of reactive free radicals (e.g., ·OH), thereby potentially catalyzing non-enzymatic browning reactions such as the Maillard reaction and Strecker degradation [33,34]. In contrast, the plane lens provides a more uniform and lower fluence density, favoring gradual molecular transformations and supporting sustained aging kinetics.

In conclusion, through multi-wavelength and multi-temporal analysis, this study demonstrates the critical role of lens geometry in DUV photocatalytic aging. Spherical lenses are optimal for short-term, high-intensity aging, whereas plane lenses are better suited for prolonged, controlled maturation. These findings provide valuable insights and a scientific foundation for developing precision optical aging technologies in Yellow Wine processing.

5. Conclusions

This study demonstrates that the spherical lens geometry, primarily through its high numerical aperture and efficient light-collecting design, significantly enhances the optical output power of DUV-LEDs by $\geq$25% compared to conventional plane lenses. This gain is realized alongside a well-managed overall optical loss within the package system. At a wavelength of 265 nm and a drive current of 30 mA, the spherical lens exhibits a pronounced optical advantage, yielding an intensity increase of 9000 a.u. relative to the plane lens—thereby offering a viable pathway for optimizing high-power DUV LED optical systems. Furthermore, experimental results reveal that the spherical lens reduces the junction temperature by 2–3 °C through improved thermal resistance. According to Arrhenius-based reliability modeling, this temperature reduction can extend device lifetime by more than 15%, underscoring its practical significance for applications requiring prolonged operation, such as disinfection and water purification.

After 1000 h of aging tests, the AlN ceramic substrate-based packaging displayed notable thermal stability, with junction temperature variation constrained within 0–1 °C. Nevertheless, optical output declined by 4–22%, which is attributed primarily to electrode oxidation. Thus, enhancing packaging hermeticity represents a critical direction for future research aimed at improving overall device longevity.

In the context of Hua Diao Yellow Wine aging, spherical lenses—owing to their higher optical output—achieved optimum aging outcomes within 20 days. However, extended irradiation to 30 days led to reduced efficacy, suggesting potential over-aging. In contrast, plane lenses produced more stable and linear aging performance. These results support a dual-strategy approach for the Yellow Wine industry: spherical lenses can enable rapid, short-term maturation, whereas plane lenses are better suited to controlled, long-term aging processes that prioritize quality consistency.

Author Contributions: Conceptualization, J.S. and J.Z.; Methodology, J.S. and Y.L.; Validation, T.W., P.W. and Y.L.; Formal analysis, J.S.; Investigation, J.S., T.W., P.W. and Y.L.; Resources, T.W., P.W. and Y.L.; Data curation, J.S. and P.W.; Writing—original draft, J.S.; Writing—review & editing, T.W. and J.Z.; Supervision, J.Z.; Project administration, J.Z.; Funding acquisition, J.Z. All authors have read and agreed to the published version of the manuscript.

Funding: R&D Program of Jiangsu Province (Grant No. BE2023048).

Data Availability Statement: Data underlying the results presented in this paper are not publicly available at this time but may be obtained from the authors upon reasonable request.

Conflicts of Interest: Authors Peng Wu and Yitao Liao were employed by the company Liyu Advanced Technology Co. Ltd. The remaining authors declare that the research was conducted in the absence of any commercial or financial relationships that could be construed as a potential conflict of interest.

References

1. Zheng, Z.; Chen, Q.; Dai, J.; Wang, A.; Liang, R.; Zhang, Y.; Shan, M.; Wu, F.; Zhang, W.; Chen, C.; et al. Enhanced light extraction efficiency via double nano-pattern arrays for high-efficiency deep UV LEDs. *Opt. Laser Technol.* **2021**, *143*, 107360. [CrossRef]
2. Floyd, R.; Gaevski, M.; Hussain, K.; Mamun, A.; Chandrashekhar, M.; Simin, G.; Khan, A. Enhanced light extraction efficiency of micropixel geometry AlGaN DUV light-emitting diodes. *Appl. Phys. Express* **2021**, *14*, 084002. [CrossRef]
3. Wan, H.; Zhou, S.; Lan, S.; Gui, C. Light extraction efficiency optimization of AlGaN-based deep-ultraviolet light-emitting diodes. *ECS J. Solid State Sci. Technol.* **2020**, *9*, 046002. [CrossRef]
4. Zhang, J.; Chang, L.; Zheng, Y.; Chu, C.; Tian, K.; Fan, C.; Zhang, Y.; Zhang, Z.-H. Integrating remote reflector and air cavity into inclined sidewalls to enhance the light extraction efficiency for AlGaN-based DUV LEDs. *Opt. Express* **2020**, *28*, 17035–17046. [CrossRef]
5. Zhang, G.; Shao, H.; Zhang, M.; Zhao, Z.; Chu, C.; Tian, K.; Fan, C.; Zhang, Y.; Zhang, Z.-H. Enhancing the light extraction efficiency for AlGaN-based DUV LEDs with a laterally over-etched p-GaN layer at the top of truncated cones. *Opt. Express* **2021**, *29*, 30532–30542. [CrossRef] [PubMed]
6. Ding, Y.; Xu, L.; Wang, Q.; Liang, R.; Peng, Y.; Wang, X.; Dai, J.; Chen, M. Heat dissipation enhancement of high-power deep-ultraviolet LEDs through plated copper on thick film diamond substrates. *IEEE Electron Device Lett.* **2024**, *45*, 1634–1637. [CrossRef]
7. Chiba, H.; Suzuki, Y.; Yasuda, Y.; Gong, T.; Tanaka, S. DUV-LED packaging using high-density TSV in silicon cavity and laser-glass-frit-bonded UV transmitting glass cap. *Sens. Actuators A Phys.* **2022**, *344*, 113700. [CrossRef]
8. Shoemaker, D.C.; Karim, A.; Kendig, D.; Kim, H.; Choi, S. Deep-Ultraviolet Thermoreflectance Thermal Imaging of GaN High Electron Mobility Transistors. In Proceedings of the 2022 21st IEEE Intersociety Conference on Thermal and Thermomechanical Phenomena in Electronic Systems (iTherm), San Diego, CA, USA, 31 May–3 June 2022; IEEE: New York, NY, USA, 2022.
9. Shen, J.; Wu, T.; Zou, J.; Wu, P.; Liao, Y. Development of deep ultraviolet LED packaging. *J. Opt. Photonics Res.* **2025**, *2*, 1–10. [CrossRef]
10. Li, Z.; Shen, M.-C.; Lai, S.; Zheng, L.; Dai, Y.; Lu, T.; Lin, S.-H.; Peng, K.; Chen, G.; Chen, Z.; et al. Enhanced Performance of AlGaN-Based DUV-LEDs With Passivated Nano-Hole Arrays. *IEEE Trans. Electron Devices* **2024**, *71*, 3722–3726. [CrossRef]
11. Lin, H.; Huang, H.; Wan, C.; Xie, Z.; Wang, H. Enhancement of radiation efficiency for DUV-LEDs by AlN-doped silicone layer filled chip-side. *IEEE Photonics Technol. Lett.* **2023**, *35*, 939–942. [CrossRef]
12. Peng, Q.; Zheng, H.; Meng, K.; Zhu, Y.; Zhu, W.; Zhu, H.; Shen, C.; Fu, J.; Elsheery, N.L.; Xie, G.; et al. The way of Qu-making significantly affected the volatile flavor compounds in Huangjiu (Chinese rice wine) during different brewing stages. *Food Sci. Nutr.* **2022**, *10*, 2255–2270. [CrossRef] [PubMed]
13. Zhang, J.; Li, T.; Zou, G.; Wei, Y.; Qu, L. Advancements and future directions in yellow rice wine production research. *Fermentation* **2024**, *10*, 40. [CrossRef]
14. Ko, Y.-S.; Kim, J.W.; Lee, J.A.; Han, T.; Kim, G.B.; Park, J.E.; Lee, S.Y. Tools and strategies of systems metabolic engineering for the development of microbial cell factories for chemical production. *Chem. Soc. Rev.* **2020**, *49*, 4615–4636. [CrossRef] [PubMed]
15. Zhao, W.; Qian, M.; Dong, H.; Liu, X.; Bai, W.; Liu, G.; Lv, X.-C. Effect of Hong Qu on the flavor and quality of Hakka yellow rice wine (Huangjiu) produced in Southern China. *LWT* **2022**, *160*, 113264. [CrossRef]
16. Badar, I.; Yang, L.; Hellmann, C.; Wyrowski, F. Freeform surface for light shaping by iterative design via Fourier domain. *Opt. Express* **2021**, *29*, 31270–31282. [CrossRef]
17. Van Roosmalen, A.H.; Anthonissen, M.J.H.; Ijzerman, W.L.; Boonkkamp, J.H.M.T.T. Fresnel reflections in inverse freeform lens design. *J. Opt. Soc. Am. A* **2022**, *39*, 1045–1052. [CrossRef]

18. Romijn, L.B.; Boonkkamp, J.H.M.T.T.; Ijzerman, W.L. Freeform lens design for a point source and far-field target. *J. Opt. Soc. Am. A* **2019**, *36*, 1926–1939. [CrossRef]
19. Truong, M.-T.; Do, P.; Mendizabal, L.; Iung, B. An improved accelerated degradation model for LED reliability assessment with self-heating impacts. *Microelectron. Reliab.* **2022**, *128*, 114428. [CrossRef]
20. Tan, K.-Z.; Lee, S.-K.; Low, H.-C. LED lifetime prediction under thermal-electrical stress. *IEEE Trans. Device Mater. Reliab.* **2021**, *21*, 310–319. [CrossRef]
21. Truong, M.-T.; Mendizabal, L.; Do, P.; Iung, B. A novel degradation model for LED reliability assessment with accelerated stress and self-heating consideration. In Proceedings of the 2021 IEEE 71st Electronic Components and Technology Conference (ECTC), San Diego, CA, USA, 1 June–4 July 2021; IEEE: New York, NY, USA, 2021.
22. Gong, R.; Wang, J.; Liu, S.; Dong, Z.; Yu, M.; Wen, C.P.; Cai, Y.; Zhang, B. Analysis of surface roughness in Ti/Al/Ni/Au Ohmic contact to AlGaN/GaN high electron mobility transistors. *Appl. Phys. Lett.* **2010**, *97*, 5588. [CrossRef]
23. Liang, S.; Sun, W. Recent advances in packaging technologies of AlGaN-based deep ultraviolet light-emitting diodes. *Adv. Mater. Technol.* **2022**, *7*, 2101502. [CrossRef]
24. Letson, B.C.; Conklin, J.W.; Wass, P.; Barke, S.; Mueller, G.; Rasel, M.A.J.; Haque, A.; Pearton, S.J.; Ren, F. Reliability and degradation mechanisms of deep UV AlGaN LEDs. *ECS J. Solid State Sci. Technol.* **2023**, *12*, 066002. [CrossRef]
25. Zhang, H.; Zhang, W.; Zhang, S.; Shan, M.; Zheng, Z.; Wang, A.; Xu, L.; Wu, F.; Dai, J.; Chen, C. Improved reliability of AlGaN-based deep ultraviolet LED with modified reflective N-type electrode. *IEEE Electron Device Lett.* **2021**, *42*, 978–981. [CrossRef]
26. Xu, F.J.; Shen, B. Progress in high crystalline quality AlNgrown on sapphire for high-efficiency deep ultraviolet light-emitting diodes. *Jpn. J. Appl. Phys.* **2022**, *61*, 040502. [CrossRef]
27. Khan, A.; Kneissl, M.; Amano, H. UV/DUV light emitters. *Appl. Phys. Lett.* **2023**, *123*, 120401. [CrossRef]
28. Liu, J.; Liu, J.; Li, S.; Cheng, H.; Lei, Z.; Peng, Y.; Chen, M. Deep-ultraviolet LEDs with all-inorganic and hermetic packaging by 3D ceramic substrate. *IEEE Photonics Technol. Lett.* **2021**, *33*, 205–208. [CrossRef]
29. Zheng, P. High Temperature Electronics Packaging Processes and Materials Development. Ph.D. Thesis, Auburn University, Auburn, AL, USA, 2010.
30. Ishii, R.; Yoshikawa, A.; Nagase, K.; Funato, M.; Kawakami, Y. Temperature-dependent electroluminescence study on 265-nm AlGaN-based deep-ultraviolet light-emitting diodes grown on AlN substrates. *AIP Adv.* **2020**, *10*, 125014. [CrossRef]
31. Lee, D.; Lee, J.W.; Jang, J.; Shin, I.-S.; Jin, L.; Park, J.H.; Kim, J.; Lee, J.; Noh, H.-S.; Kim, Y.-I. Improved performance of AlGaN-based deep ultraviolet light-emitting diodes with nano-patterned AlN/sapphire substrates. *Appl. Phys. Lett.* **2017**, *110*, 191103. [CrossRef]
32. Chen, Z.; Liu, Z.; Wei, T.; Yang, S.; Dou, Z.; Wang, Y.; Ci, H.; Chang, H.; Qi, Y.; Yan, J.; et al. Improved epitaxy of AlN film for deep-ultraviolet light-emitting diodes enabled by graphene. *Adv. Mater.* **2019**, *31*, 1807345. [CrossRef]
33. Charnock Hannah, M.; Pickering, G.J.; Kemp, B.S. The Maillard reaction in the traditional method of sparkling Yellow Wine. *Front. Microbiol.* **2022**, *13*, 979866.
34. Ma, T.; Wang, J.; Wang, H.; Zhao, Q.; Zhang, F.; Ge, Q.; Li, C.; Gamboa, G.G.; Fang, Y.; Sun, X. Yellow Wine aging and artificial simulated Yellow Wine aging: Technologies, applications, challenges, and perspectives. *Food Res. Int.* **2022**, *153*, 110953. [CrossRef]